TRANSPARENT PROCESS

OPEN ACCESS

EMBO *reports*

# Mobile late endosomes modulate peripheral endoplasmic reticulum network architecture

Menno Spits, Iris T Heesterbeek, Lennard M Voortman, Jimmy J Akkermans, Ruud H Wijdeven, Birol Cabukusta[*] iD & Jacques Neefjes[**] iD

## Abstract

**The endoplasmic reticulum (ER) is the largest organelle contacting virtually every other organelle for information exchange and control of processes such as transport, fusion, and fission. Here, we studied the role of the other organelles on ER network architecture in the cell periphery. We show that the co-migration of the ER with other organelles, called ER hitchhiking facilitated by late endosomes and lysosomes is a major mechanism controlling ER network architecture. When hitchhiking occurs, emerging ER structures may fuse with the existing ER tubules to alter the local ER architecture. This couples late endosomal/lysosomal positioning and mobility to ER network architecture. Conditions restricting late endosomal movement—including cell starvation—or the depletion of tether proteins that link the ER to late endosomes reduce ER dynamics and limit the complexity of the peripheral ER network architecture. This indicates that among many factors, the ER is controlled by late endosomal movement resulting in an alteration of the ER network architecture.**

## Introduction

The endoplasmic reticulum (ER) is the largest intracellular membrane compartment with a complex architecture covering most cellular space outside the nucleus and interacting with every other organelle and the plasma membrane. The ER functions as a multifunctional platform mediating a plethora of biological processes, such as lipid synthesis, protein production and folding, controlling calcium homeostasis, and antigen presentation for immune surveillance (Elliott & Neefjes, 2006; Raffaello *et al*, 2016). The ER interacts with other organelles by forming molecular bridges and creating membrane contact sites (MCS) (Rowland *et al*, 2014; Hoyer *et al*, 2018). At MCS, the ER exchanges information and metabolites, such as cholesterol and calcium, between organelles. Overall, the ER controls many intracellular processes.

The ER forms a complex network structure with subdomains in the form of tubules and sheets, linked with junctions to generate its characteristic netted shape. This complex ER architecture is created and maintained through a wide range of proteins and lipids. Formation of membrane curvature and tubule formation requires proteins containing reticulon homology domains, which have a characteristic hairpin-like transmembrane structure (Wang *et al*, 2016; Bhaskara *et al*, 2019). Meanwhile, three-way ER junctions are formed by Atlastin-1 homodimers on opposing ER membranes orchestrating homotypic fusion. Following membrane fusion, Lunapark localizes to the nascent junctions to stabilize the unique inward curvature of the junction (Goyal & Blackstone, 2013; Chen *et al*, 2015; Wang *et al*, 2016; Zhou *et al*, 2019).

The architecture of the ER is highly dynamic and undergoes constant remodeling (Guo *et al*, 2018; Zhou *et al*, 2019). Two mechanisms of ER movement have been described. In the first mechanism, the tip attachment complex (TAC)-mediated ER movement, the ER-resident protein STIM1 interacts with EB1 at the microtubule plus-end and a new ER tubule travels alongside the polymerizing microtubule. Overexpression of STIM1 or inhibiting (de)polymerization of the microtubules results in an ER structure strongly resembling the shape of the microtubule network structure (Grigoriev *et al*, 2008; English *et al*, 2009). The second mechanism, named ER sliding occurs through the direct interaction between the motor protein Kinesin-1 and the ER protein Kinectin allowing the ER to expand in the plus-end direction of microtubules (Santama *et al*, 2004; Lin *et al*, 2012; Goyal & Blackstone, 2013). In parallel, a recently described third way of ER movement called ER hitchhiking demonstrated that ER tubules co-migrate with an associated organelle (Salogiannis & Reck-Peterson, 2017; Guo *et al*, 2018; Mogre *et al*, 2020). Here, ER tubules are being drawn forward by an associated organelle such as peroxisomes or lipid droplets, copying its mobility (Zajac *et al*, 2013; Guimaraes *et al*, 2015; Salogiannis *et al*, 2016). However, the frequency and nature of ER hitchhiking events and their relation to previously described ER movement mechanisms are unclear.

To investigate endosome-related ER hitchhiking and to understand the relationship between ER movement and endosomal

Division of Cell and Chemical Biology, Oncode Institute, Leiden University Medical Centre, Leiden, The Netherlands
*Corresponding author. Tel: +31 71 5268724; E-mail: b.cabukusta@lumc.nl
**Corresponding author. Tel: +31 71 5268722; E-mail: j.j.c.neefjes@lumc.nl

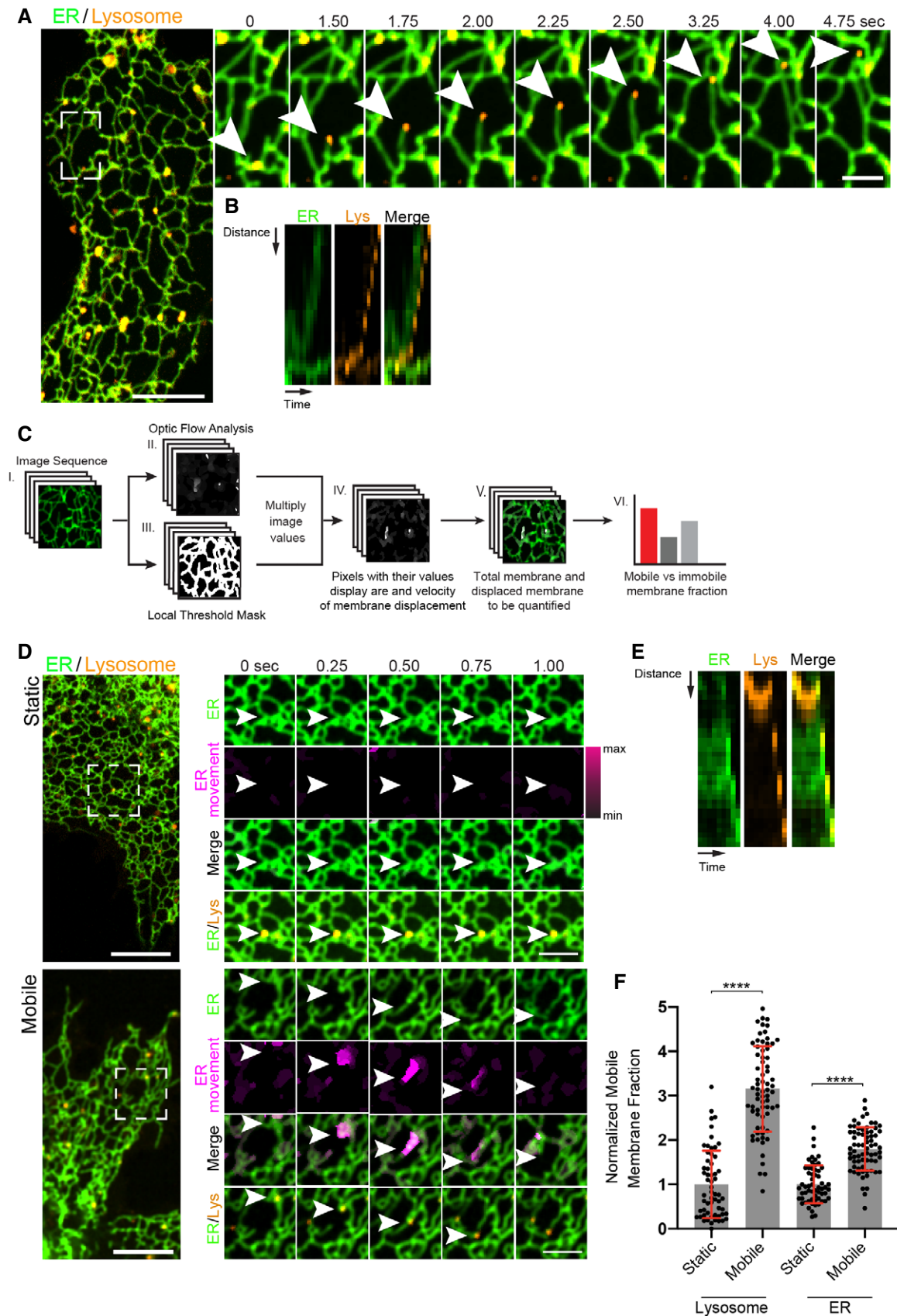*EMBO reports* 22: e50815 | 2021    **1 of 14**

Figure 1.

◀

**Figure 1. Motility of late endosomes/lysosomes and the ER network.**

A  Representative time-lapse spinning disk confocal images of *n* = 3 of live COS7 cells stably expressing ER marker GFP-TMD (green). The cells were loaded with SiR-lysosome to visualize LE/Lys (orange). Zoom insets show a merge of the ER (GFP-TMD) (green) and SiR-lysosome labeled LE/Lys (orange). Zoom insets show a region of interest containing a mobile endosome as denoted by the white arrow. Scale bars: full size 10 μm, zoom inset 3 μm. Images related to Movie EV1.

B  Kymograph of the representative image in panel (A).

C  Schematic flow of membrane displacement analysis method.

D  Representative time-lapse spinning disk confocal images of *n* = 3 of COS7 cells stably expressing GFP-TMD (ER) (green) and SiR-lysosome (orange). Zoom insets highlight regions of interest containing a static (upper panels) or mobile endosome (lower panels) as denoted by the white arrows. First row shows ER (green), the second row shows MDA-generated ER movement (magenta), third row shows a merge of the two channels, and the fourth row shows a merge of ER (green) and LE/Lys (orange). Scale bars: full size 10 μm, zoom inset 3 μm. Images relate to Movies EV2 and EV3.

E  Kymograph of the mobile vesicle in panel (D).

F  MDA quantification of (D). Mobility of static and mobile endosomes was quantified and normalized to the static endosomes. Graph represents mean ± s.d. of analyses at multiple locations within the same cell(*n* = 20 cells per condition from 3 independent experiments). All images acquired for 90 frames at 4Hz. Significance two-tailed Student *t*-test, ****$P < 0.0001$.

movement, we developed a method to quantify ER movement in association with other membrane structures. With this tool, we observed that ER hitchhiking occurs with various types of endosomes, but preferably RAB7-marked late endosomes and lysosomes (LE/Ly). We show that late endosomal ER hitchhiking occurs independent of TAC-mediated ER movement or ER sliding and contributes to half of all ER movements in COS7 cells. Reducing late endosomal transport by starvation or introducing factors driving LE/Ly to the microtubule minus-end to remove them from the cell periphery also limits ER hitchhiking and results in a less complex and more open ER network in the cell periphery. Depletion of MCS proteins that tether the ER to LE/Ly, the ER-resident VAP proteins, significantly reduced ER hitchhiking events, suggesting a novel function of ER-LE/Ly contact sites. We propose that late endosomal mobility in the cell periphery is a major contributor to the formation and maintenance of the local ER network architecture.

## Results

### Mobile late endosomes/lysosomes and ER movement

To assess the contribution of endosomes on ER movement, we marked the ER by fusing eGFP to the *N*-terminal cytosolic tail of the transmembrane region of the ER-localized MOSPD2 or with mCherry-KDEL (Di Mattia *et al*, 2018). COS7 cells stably expressing these constructs were used in our experiments. We visualized LE/Ly with the lysosome-specific fluorophore SiR-lysosome. The behavior of the ER relative to the LE/Ly compartment was imaged using parallel high-speed acquisition by a spinning disk confocal microscope. We observed movements suggesting that LE/Ly co-migrate with ER tubules. This was further illustrated by the accompanying kymograph (Fig 1A and B, Movie EV1) and is in line with previous observations (Guimaraes *et al*, 2015; Salogiannis *et al*, 2016; Guo *et al*, 2018). Notably, these movements often appeared to yield novel ER network junctions. Following the formation of new junctions, 78% of the observed vesicle-ER tubule pairs resume with their co-migration. To examine whether the LE/Ly co-migration with ER tubules, so-called ER hitchhiking events, involve the leading tip of dynamic ER tubules, we used CEPT1 and PIS, two previously described markers for these ER subdomains (English & Voeltz, 2013). Protein localizations during hitchhiking events revealed that PIS and CEPT1 are indeed enriched in 78% and 80% of the hitchhiking events, respectively

(Fig EV1A and B, Movies EV4 and EV5). This suggests that ER hitchhiking events mainly take place at the leading edge of dynamic ER tubules.

To quantify ER hitchhiking processes, a method was developed for automated image analysis. The available analyses methods—such as particle tracking and network analysis—are unable to accurately quantify the membrane displacement of heterogeneously shaped membranes such as the ER. Therefore, we developed a membrane displacement analysis (MDA) method based on optical flow analysis (Horne, 1981) (Fig 1C). This tool allowed us to accurately assess the movement fraction of any fluorescently labeled membrane and captured any detectable motion without requiring an *a priori* accurate and reliable localization of points of interest.

Using MDA, we analyzed image sequences acquired at 4Hz at multiple areas of 36 μm² per cell, in a range of cells, as an accurate representation of membrane structures moving in relation to each other. We discerned differences in ER movement surrounding static late endosomes and mobile late endosomes (Fig 1D–F, Movies EV2 and EV3). This revealed a 1.8-fold increase of ER movement surrounding mobile late endosome (Fig 1F). Thus, MDA showed a significant increase in ER movement when LE/Ly moved through the focused area and suggests that LE/Ly are involved in ER dynamics. Furthermore, we observed that 80% of the hitchhiking events continue to interact with the ER following apparent ER network formation (Fig EV1C), suggesting the absence of a specific hitchhiking termination following these events.

### ER hitchhiking occurs independently of TAC-mediated ER movement and ER sliding

Two mechanisms of ER mobility have been reported: TAC-mediated ER movement and ER sliding (Fig 2A). We assessed whether these mechanisms could explain ER hitchhiking with LE/Ly. To study the role of TAC-mediated ER movement, we evaluated ER hitchhiking occurring along polymerizing microtubules in cells expressing EB3-GFP, which selectively marks growing microtubules (van de Willige *et al*, 2016). An ER tubule following a late endosome was often detected in the absence of any nearby EB3-GFP signal (Fig 2B, Movie EV6). To further determine the contribution of growing microtubules in ER hitchhiking, we exposed cells to paclitaxel, which blocks microtubule polymerization therefore abolishes TAC-mediated ER movement (Horwitz, 1994). As expected, paclitaxel treatment reduced the
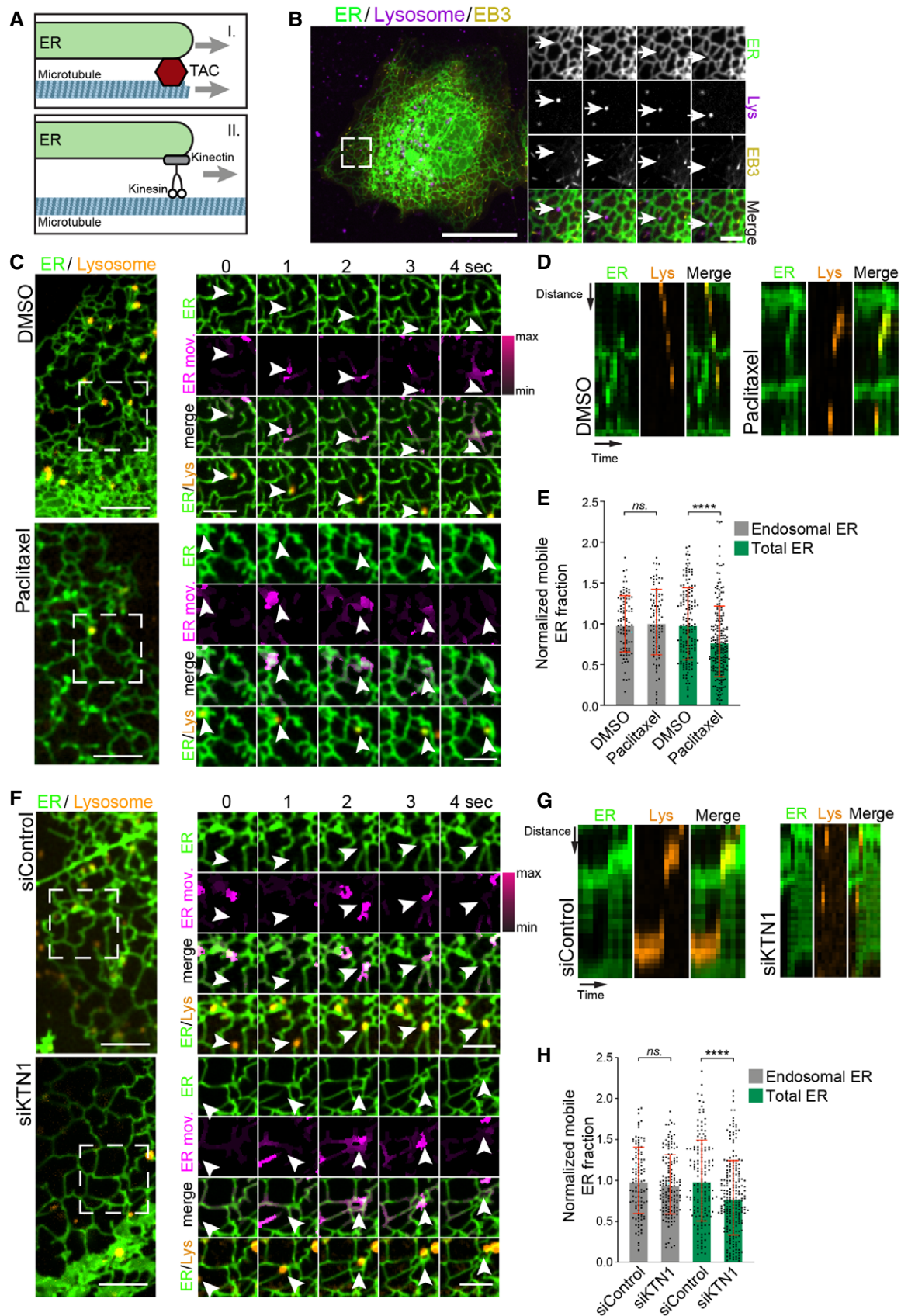
Figure 2.

**Figure 2.  ER hitchhiking and other processes of ER movement.**

A   Schematic representation of TAC-mediated (I) ER movement and ER sliding (II).
B   Representative time-lapse spinning disk confocal images of *n* = 3 of live COS7 cells stably expressing mCherry-KDEL (green), transiently expressing EB3-GFP (yellow), and SiR-lysosome-stained LE/Lys (magenta). Zoom insets show regions of interest containing a mobile LE/Lys as denoted by the white arrow. First row shows ER (mCherry-KDEL) (green), the second row shows SiR-lysosome-stained LE/Lys (magenta), the third row shows EB3-GFP (yellow) and the fourth row shows the merge of the three preceding channels. Scale bar: 30 μm and zoom insets 3 μm. All images acquired for 90 frames at 1Hz. Images related to Movie EV6.
C   Representative time-lapse spinning disk confocal images of *n* = 3 of live COS7 cells stably expressing GFP-TMD (green) marked ER and SiR-lysosome-stained LE/Lys (orange). Zoom insets highlight regions of interest containing a mobile endosome as denoted by the white arrow. First row represents ER (GFP-TMD) (green), the second row shows MDA-generated ER movement (magenta), third row shows a merge of the two preceding channels, and the fourth row shows a merge of ER (green) and LE/Lys (orange). Samples were treated with either DMSO or 2 μM paclitaxel. Scale bar: 30 μm and zoom insets 3 μm. All images acquired for 90 frames at 1Hz. Images related to Movie EV7 and EV8.
D   Kymograph of panel (C).
E   MDA quantification of panel (C) normalized to control cells, showing the average ER movement surrounding LE/Lys under control or treated conditions and the overall average ER mobility under control or treatment conditions. Graph represents mean ± s.d. of analyses at multiple locations within the same cell (*n* = 20 cells per condition from 3 independent experiments). Significance two-tailed Student *t*-test ****$P$ < 0.0001; ns = not significant.
F   Representative images of *n* = 3 of COS7 cells stably expressing GFP-TMD (green) to mark the ER and SiR-lysosome stained LE/Lys (orange) merged. Zoom insets highlight region of interest containing a mobile endosome as denoted by the white arrow. First row represents ER (GFP-TMD) (green), the second row shows MDA-generated ER movement (magenta), third row shows a merge of the two preceding channels, and the fourth row shows a merge of ER (green) and LE/Lys (orange). Samples were treated with either siControl or siKTN1. Scale bar: 30 μm and zoom insets 3 μm. All images acquired for 90 frames at 1Hz. Images related to Movies EV9 and EV10.
G   Kymograph of panel (F).
H   MDA quantification of panel (F) normalized to control cells, showing the average ER movement surrounding LE/Lys under control or treated conditions and the overall average ER mobility under control or treatment conditions, respectively. Graph represents mean ± s.d. of analyses at multiple locations within the same cell (*n* = 20 cells per condition from 3 independent experiments). Significance two-tailed Student *t*-test. ****$P$ < 0.0001; ns = not significant.

total ER mobility significantly; however, it failed to affect local ER movements connected to mobile LE/Ly (Fig 2C–E, Movie EV7 and EV8). Alternatively, ER sliding is responsible for the ER movement observed during ER hitchhiking events. ER sliding is facilitated by the ER-resident protein Kinectin interacting with the microtubule motor Kinesin-1 (Santama *et al*, 2004; Friedman *et al*, 2010; Lin *et al*, 2012; Goyal & Blackstone, 2013; Chen *et al*, 2015). To assess this possibility, cells were depleted of Kinectin and analyzed by time-lapse microscopy (Fig EV1D and E). MDA confirmed that Kinectin-depleted cells demonstrated reduced total ER movement. But the ER movement surrounding LE/Ly hitchhiking events remained unaffected (Fig 2F–H, Movies EV9 and EV10). These data confirm that TAC-mediated ER movement and ER sliding contribute significantly to the total ER movement, but also suggest that ER hitchhiking with LE/Ly occurs independently of these two mechanisms.

## ER hitchhiking mainly involves peripheral mobile RAB7-marked late endosomes that are manipulated by TMEM55B and starvation

We wondered whether all endosomal structures contribute to ER hitchhiking or whether RAB7-marked LE/Ly are the main contributors. For this, various endosomes were marked by GFP-labeled RAB GTPases: RAB5 for early endosomes, RAB11 and RAB14 for recycling endosomes, and RAB7 for LE/Ly (Ullrich *et al*, 1996; Jordens *et al*, 2001; Junutula *et al*, 2004; Rocha *et al*, 2009; Friedman *et al*, 2013; Wijdeven *et al*, 2016; Bakker *et al*, 2017; Langemeyer *et al*, 2018; Zulkefli *et al*, 2019). We used MDA to quantify ER movement associated with the movement of each endosomal population. Mobile RAB5, RAB11, and RAB14 mobility were all associated to an average of 1.2-fold increase in ER mobility in the analyzed areas compared to their static counterparts (Fig 3C, Fig EV2A–F, Movies EV13–EV18).

**Figure 3.  RAB7-positive endosomes and ER mobility.**

A   Representative time-lapse spinning disk confocal images of *n* = 3 live COS7 cells stably expressing mCherry-KDEL (green) and transiently expressing GFP-RAB7 (orange). Zoom insets show a region of interest containing a mobile RAB7-positive endosome as denoted by the white arrows. First row represents the ER (mCherry-KDEL) (green), the second row shows MDA-generated ER movement (magenta), third row shows a merge of the two preceding channels, and the fourth row shows a merge of ER (green) and GFP-RAB7 (orange). Scale bar: 10 μm, zoom insets 3 μm. Images related to Movie EV11. Images were acquired for 90 frames at 1Hz.
B   Kymograph of panel (A).
C   MDA quantification of panel (A) and Fig EV2A–G normalized to 1 showing average ER movement surrounding static endosomes and mobile endosomes. Graph represents mean ± s.d. of analyses at multiple locations within the same cell (*n* = 15 cells per condition from 3 independent experiments). All images acquired for 90 frames at 1Hz. Significance two-tailed Student *t*-test. *$P$ < 0.05, **$P$ < 0.01, ****$P$ < 0.0001 ns = not significant.
D   Violin plots of fractional distance analysis showing the average distribution of endosomes in cells from panel (E) and Fig EV3A. Graph represents mean ± s.d. of *n* = 15 cells per condition from 3 independent experiments. Dashed lines represent median and solid lines represent interquartile range. Cartoons representing the overexpression and control LE/Ly phenotype. Significance two-tailed Student *t*-test. ****$P$ < 0.0001.
E   Representative time-lapse spinning disk confocal images of *n* = 3 of live COS7 cells stably expressing GFP-TMD (green) and in lower panels transiently expressing mScarlet-RILP (magenta) and SiR-lysosome-stained LE/Lys (orange). Zoom insets shows region of interest containing ER (GFP-TMD). First row represents ER (GFP-TMD) (green), the second row shows MDA-generated ER movement (magenta), and third row shows a merge of the two preceding channels. Scale bar: 10 μm, zoom insets 3 μm. Images related to Movie EV19 and Movie EV20. Images were acquired for 90 frames at 1Hz.
F   MDA quantification of panel (E) and Fig EV3A normalized to 1 showing total average ER movement. Graph represents mean ± s.d. of analyses at multiple locations within the same cell (*n* = 15 cells per condition from 3 independent experiments). All images acquired 90 frames at 1Hz. Significance two-tailed Student *t*-test. ****$P$ < 0.0001 ns = not significant.
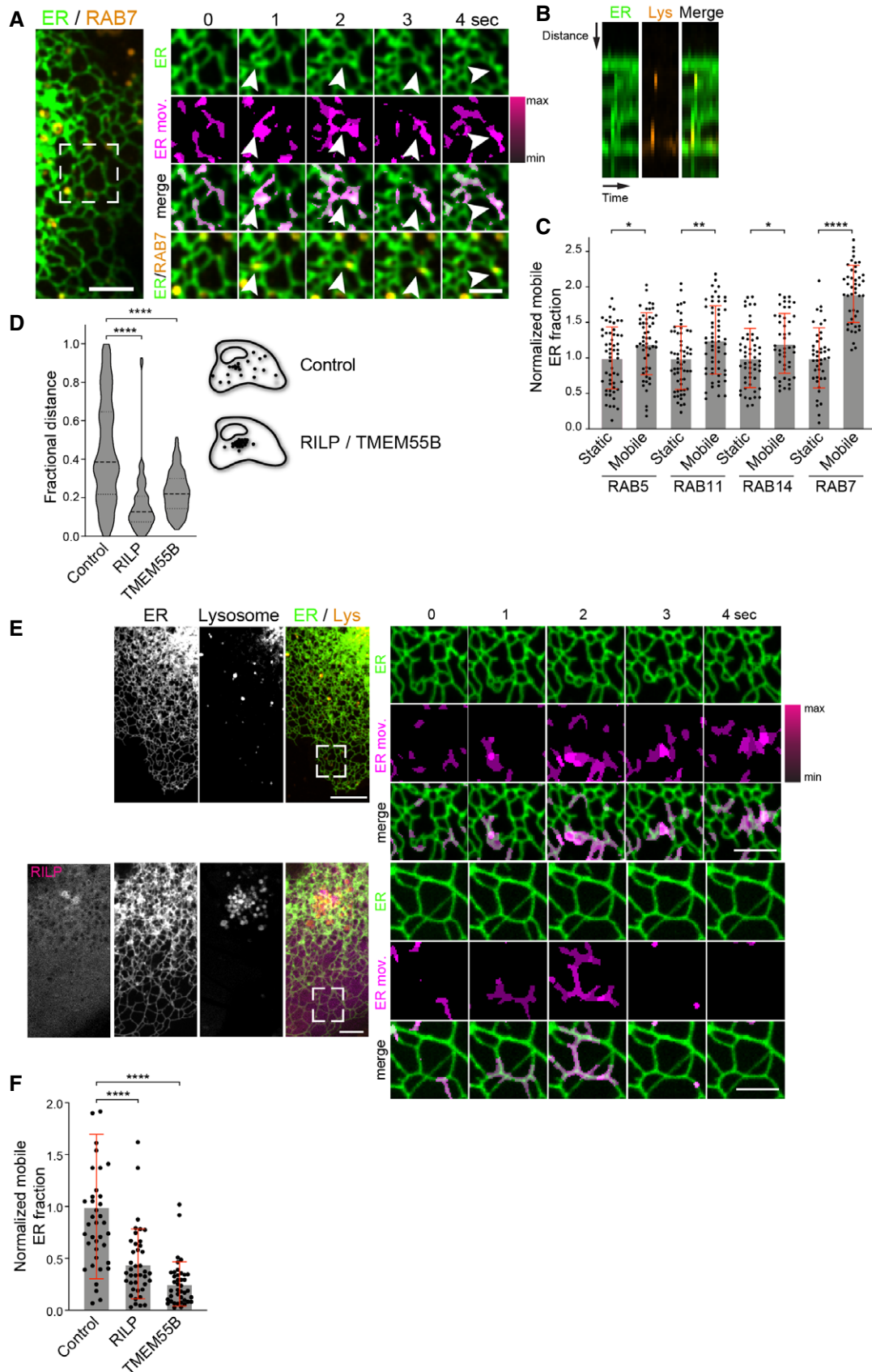
Figure 3.

Mobile RAB7 demonstrated a 2-fold increase in ER mobility compared to its static counterparts (Fig 3A–C, Fig EV2G, Movies EV11 and EV12). Meanwhile, overexpression of RABs did not influence the overall mobility of ER or vesicles, or caused aberrant changes in the peripheral ER architecture (Fig EV2H–K). This suggests that RAB7-positive LE/Ly contribute to ER hitchhiking significantly more than the other endosomal compartments tested.

To assess the overall contribution of LE/Ly transport to ER movement, we blocked their mobility by relocating these structures to the microtubule minus-end close to the microtubule-organizing center (MTOC) and thus avert their presence in the cell periphery. This was accomplished by overexpressing either the RAB7 effector RAB-interacting lysosomal protein (RILP) or the phosphatidylinositol-4,5-biphosphate 4-phosphatase (TMEM55B). RILP recruits p150[glued] and hereby the dynein motor to LE/Ly. TMEM55B localizes in LE/Ly and binds to JIP4 which then recruits the dynein motor. Recruitment of dynein to LE/Ly by RILP or TMEM55B leads to minus-end transport and their clustering in the perinuclear region (Jordens et al, 2001; Rocha et al, 2009; Wijdeven et al, 2016; Willett et al, 2017; Cabukusta & Neefjes, 2018). Indeed, overexpression of RILP or TMEM55B resulted in a characteristic LE/Ly clustering phenotype (Fig 3D). We performed MDA on ER movement in these cells in fields of 36 $\mu m^2$ at various locations in order to capture the average motility of the ER alone. This yielded an average reduction of 50% in overall ER movement in cells overexpressing RILP and 60% in cells overexpressing TMEM55B relative to control samples (Fig 3E–F, Fig EV3A, Movies EV19–EV21). Of note, overexpression of RILP or TMEM55B was selective for LE/Ly and did not reduce the movement of mitochondria, peroxisomes or RAB5-positive vesicles (Fig EV3B–D, Movies EV22–EV29). It appears that constraining LE/Ly transport significantly reduces total ER mobility.

Interestingly, TMEM55B connects late endosomal transport to the metabolic state of cells: Cells undergoing starvation upregulate TMEM55B expression to sequester the LE/Ly in the perinuclear region around the MTOC (Willett et al, 2017). This results in LE/Ly clustering therefore restricting their motility. We thus wondered whether starvation of cells also results in reduced ER movement similar to TMEM55B overexpression. Starved cells displayed a 22% reduction in endosomal mobility and a 33% reduction in overall ER dynamics (Fig EV3E–G, Movies EV30 and EV31). Next, we wondered whether the depletion of LE/Ly from the cell periphery as a result of starvation somehow causes non-lysosomal endosomes to be more prevalent in ER hitchhiking. To this end, we examined the contribution of RAB5, RAB11, and RAB14, which previously appeared auxiliary to ER hitchhiking, to ER hitchhiking events under starvation conditions. Under starvation, the RAB7-positive endosomes, LE/Ly, displayed the most significant reduction in total vesicular movement and ER hitchhiking (Fig EV3H–I, Movies EV32–EV39). Meanwhile, the RAB5-, RAB11- or RAB14-marked endosomes did not show any additional contribution to ER hitchhiking under starvation. If anything, starvation reduced the ability of each vesicle type to generate ER movement. Collectively, our data suggest that RAB7-positive LE/Ly provide the majority of peripheral ER hitchhiking events.

### Mobile late endosomes/lysosomes design the peripheral ER network architecture as modulated by starvation

Next, we tested whether the LE/Ly-mediated ER movement had an effect on the overall architecture of the peripheral ER network. To address this, we analyzed the ER architecture by quantifying the number of ER junctions per $\mu m^2$. This was accomplished by developing a semi-automatic analysis method (Fig 4A). We observed that restricting LE/Ly mobility by overexpression of RILP or TMEM55B also decreased the number of peripheral ER junctions per $\mu m^2$, resulting in a more open ER structure (Fig 4B and C). Similar to ER mobility, the complexity of the ER network architecture was also reduced upon starvation (Fig EV3J and K). Overall, these data suggest that LE/Ly movement and ER hitchhiking contribute significantly to the overall ER architecture and explains how starvation of cells translates in a "more open" peripheral ER network.

### ER–late endosome/lysosome membrane contact site proteins facilitate ER hitchhiking

Our data suggest that LE/Ly contribute to ER mobility and ER network architecture. As previously reported, ER hitchhiking is defined as the ER tethered to another organelle propelled by a motor protein (Salogiannis & Reck-Peterson, 2017; Guo et al, 2018; Mogre et al, 2020). Accordingly, disrupting MCS between the ER and LE/Ly could diminish ER hitchhiking events with LE/Ly and consequently reduce the complexity of the peripheral ER network. To this end, we focused on the ER-resident VAP proteins, VAPA, VAPB, and MOSPD2. These proteins participate in the formation of MCS between the ER and other organelles, including LE/Ly (Murphy & Levine, 2016; Di Mattia et al, 2018). To test whether MCS proteins can be involved in ER hitchhiking, we depleted cells of these proteins (Fig EV4A–C). While the depletion of individual VAP proteins yielded a mild reduction in ER mobility, combined depletion of all three VAP proteins demonstrated the most significant decrease in ER mobility (Fig 5A, C and D, Fig EV4D–I, Movies EV40–EV47). This also corroborates a previous report where co-depletion of all three tethering proteins leads to the most significant reduction in ER-LE/Ly contact sites, most likely due to possible redundancy among VAPA, VAPB, and MOSPD2 that have an overlapping substrate specificity (Di Mattia et al, 2018). Silencing the VAP proteins did not affect total endosomal mobility or overall general ER morphology (Fig EV4J), suggesting that MCS between the ER and LE/Ly is required for ER hitchhiking with LE/Ly but not for LE/Ly trafficking (Figs 5D and Fig EV4K).

Next, we examined whether the VAP-mediated late endosomal ER hitchhiking events affect the peripheral ER network architecture. We observed that the depletion of individual VAP proteins reduces the number of peripheral ER junctions. However, triple depletion of VAP proteins showed the largest decrease (Figs 5B and E, and Fig EV5A–F), further substantiating the role of hitchhiking events in the formation of the peripheral ER architecture. Overall, our results suggest that the tether proteins facilitating ER-LE/Ly contact sites contribute to LE/Ly-mediated ER hitchhiking, which ultimately designs the peripheral ER network architecture.

## Discussion

The ER is the most extensive membranous organelle spanning the entire cytoplasm and interacting with every other compartment to exchange information and metabolites. The ER is consisting of subcompartments such as the nuclear envelope, the perinuclear region,
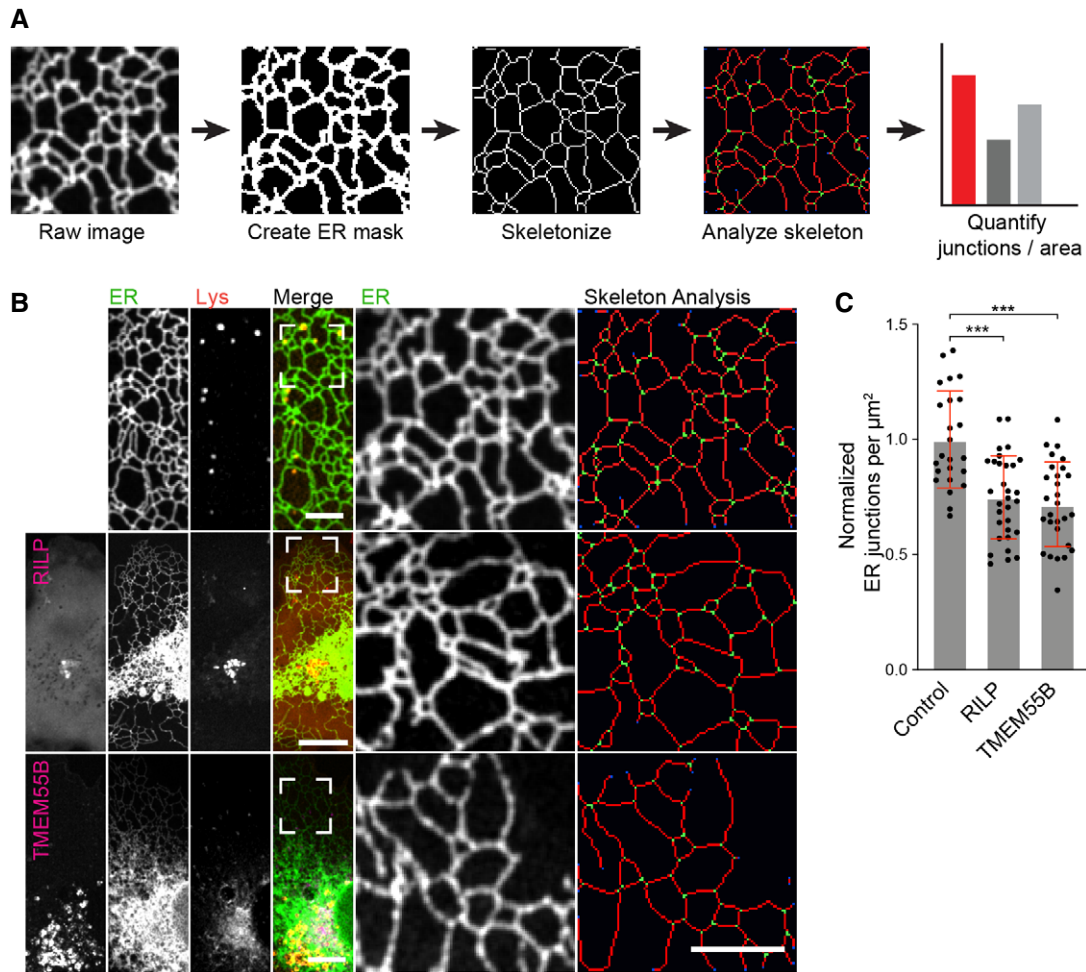
**Figure 4. Endosomal clustering reduces peripheral ER junctions.**

A   Schematic flow overview of the process for ER junction quantification.
B   Representative stills of spinning disk confocal images of $n = 3$ of COS7 cells stably expressing TMD-GFP (green) and SiR-lysosome-stained endosomes/lysosomes (orange). COS7 cells in the middle panels overexpress mCherry-RILP (magenta). The COS7 cells in the lower panels overexpress mCherry-TMEM55B (magenta). Zoom insets show region of interest containing the ER (TMD-GFP) (green) and junction analysis of the skeletonized ER where the number of ER junctions representing the quantified average. Scale bars: 15 µm. zoom insets: 3 µm.
C   Quantification of the number of ER junctions per µm$^2$ from panel (B) as resulted from ER junction analysis. Graph represents mean $\pm$ s.d. of analyses at multiple locations within one cell ($n = 15$ from 3 independent experiments). Significance two-tailed Student $t$-test. ***$P < 0.001$.

**Figure 5. ER tethers support ER hitchhiking.**

A   Representative images of time-lapse spinning disk confocal images of $n = 3$ of COS7 cells stably expressing GFP-TMD (green) and SiR-lysosome-stained LE/Lys (orange) treated with either siControl or co-treated with siVAPA, siVAPB, and siMOSPD2. Zoom insets show regions of interest containing mobile LE/Lys as denoted by the white arrow. First row represents ER (TMD-GFP) (green), the second row shows MDA-generated ER movement (magenta), third row shows a merge of the two preceding channels, and the fourth row shows a merge of ER (green) and SiR-lysosome stained LE/Lys (orange). Scale bar: 5 µm, zoom insets 3 µm. Images related to Movies EV40 and EV47. Images were acquired for 90 frames at 1Hz.
B   Representative stills of spinning disk confocal images of $n = 3$ of COS7 cells stably expressing TMD-GFP (green) and SiR-lysosome-stained endosomes/lysosomes (orange) treated with siControl or with siVAPA, siVAPB, and siMOSPD2. Zoom insets show region of interest containing ER (TMD-GFP) (green) and junction analysis of skeletonized ER where number of ER junctions representing the quantified average. Scale bars: 10 µm. zoom insets: 3 µm.
C   MDA quantification of ER of panels (A, B) and Fig EV4B–G normalized to control cells showing average ER movement surrounding mobile endosomes. Graph represents mean $\pm$ s.d. of analyses at multiple locations within the same cell ($n = 30$ cells per condition from 3 independent experiments). All images acquired for 90 frames at 1Hz. Significance two-tailed Student $t$-test. **$P < 0.01$, ****$P < 0.0001$, ns = not significant.
D   MDA quantification of SiR-lysosome-stained LE/Lys of (A, B) and Fig EV4B–G normalized to 1 showing total average endosomal movement. Graph represents mean $\pm$ s.d. of $n = 15$ cells per condition from 3 independent experiments. Significance two-tailed Student $t$-test. ns = not significant.
E   Quantification of number of ER junctions per µm$^2$ from (B) and fig. H – M as resulted from ER junction analysis. Graph represents mean $\pm$ s.d. of analyses at multiple locations within one cell of $n = 15$ from 3 independent experiments. Significance two-tailed Student $t$-test. *$P < 0.05$, **$P < 0.01$ ***$P < 0.001$, ****$P < 0.0001$, ns = not significant.

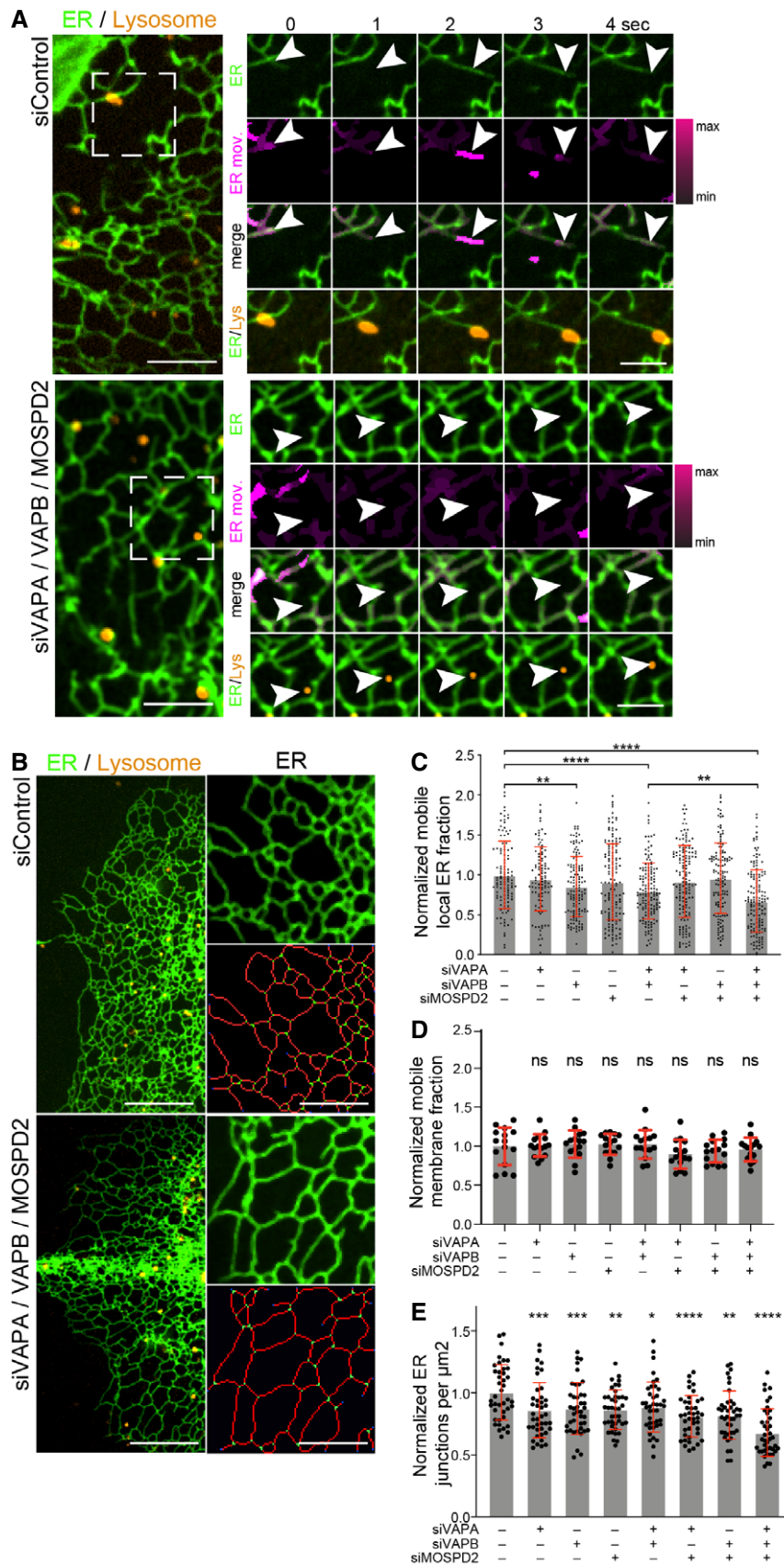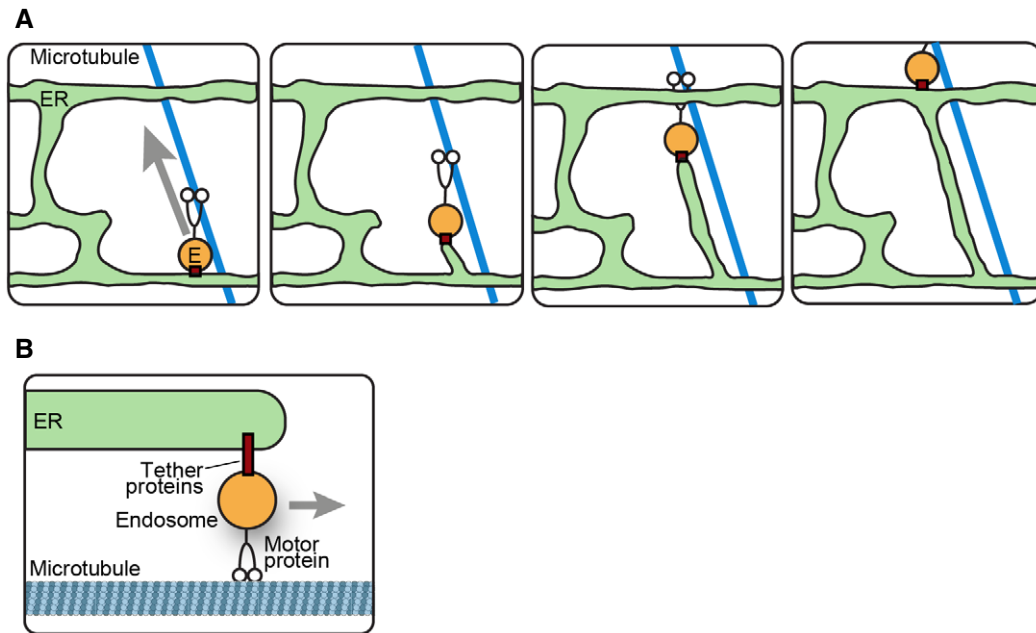**Figure 5.**

**Figure 6. Model for ER hitchhiking induced ER structuring.**

A   (1) A tethered LE/Lys initiates movement. (2) Upon movement, the tether remains intact and the ER is able to hitchhike along with the LE/Lys. (3) When the tethered pair encounter an ER tubule, junction formation may be initiated. (4) After formation the ER may remain tethered.
B   ER hitchhiking is likely facilitated by a range of ER- LE/Lys tethers yet will require motor protein recruitment to drive hitchhiking.

and the peripheral region, but the exact nature of these regions is still discussed. While the perinuclear ER is dense and difficult to distinguish by light microscopy, this is not the case for the more peripheral ER. The peripheral ER is composed of dynamic tubular structures. New tubules arise from the existing ER to build the complex interconnected ER network. This has been visualized by high-end microscopy in a study that also visualized endosomes and peroxisomes leading the formation of new ER tubules (Guo *et al*, 2018). Here, we studied the contribution of the endosomal compartments in designing the architecture of the ER (Fig 6). We used image analysis methods to quantify this contribution and show that especially RAB7-marked LE/Ly support the formation of new ER tubules through a mechanism called hitchhiking. LE/Ly then drag along associated ER tubules in their transport process, a process involving ER-located VAP proteins. Reducing LE/Ly in the peripheral regions of cells by overexpression of RILP or TMEM55B or by starvation of cells directly affects this way of ER architecture formation. As the ER affects many LE/Ly processes such as transport and fusion, LE/Ly also contributes to the ER network design (Rocha *et al*, 2009; van der Kant *et al*, 2013).

Two independent mechanisms of microtubule-mediated ER movement have been reported before: ER sliding and TAC-mediated ER movement (Grigoriev *et al*, 2008; Bola & Allan, 2009; Friedman *et al*, 2010). Here, we followed a third mechanism, ER hitchhiking with LE/Ly. Our image analyses tool allowed us to quantify the relative contribution of each process in COS7 cells. This suggested that about half of peripheral ER movements occurs by ER hitchhiking, while TAC and ER sliding each contribute around 25%. While the numbers are based on perturbations that could be incomplete and

variable under different conditions, they still define that at least three systems are contributing to the total ER tubule formation and architecture. The relative contribution of each process is likely dictated by the type of cell and physiological conditions. We observed that following an ER hitchhiking event, a protruding ER tubule dragged along by LE/Ly is capable of fusing with existing distal ER tubules to generate a novel ER junction. This suggests that the regulation of ER architecture is not an autonomous process build by LE/Ly movement. Accordingly, reducing late endosomal trafficking by RILP or TMEM55B overexpression or by starvation results in a significant reduction in LE/Ly transport in the cell periphery and a concomitantly reduced complexity of the ER architecture.

While we tested several endosomal compartments labeled by their characteristic RAB GTPases, we observed that ER movement was predominantly linked to mobile LE/Ly. This is in line with previous observations in which LE/Ly were found to be the dominant type of endosomes interacting with the ER (Friedman *et al*, 2013). Multiple protein complexes localize at MCS between the ER and LE/Ly: late endosomal ORP1L, STARD3, and STARD3NL each form molecular bridges with VAP proteins (Rocha *et al*, 2009; Di Mattia *et al*, 2018). The best characterized contacts are between the ER-localized VAPA, VAPB, and MOSPD2 (Jordens *et al*, 2001; Rocha *et al*, 2009; Wijdeven *et al*, 2016; Zhao *et al*, 2018). We found that VAPA, VAPB and MOSPD contribute to the peripheral ER hitchhiking events, as depletion of these three proteins yielded a 33% reduction in ER mobility. The remainder could be accounted for by other non-VAP-mediated contact sites, such as RNF26 and TOLLIP or Protrudin and RAB7 (Jongsma *et al*, 2016; Raiborg *et al*, 2016).

ER hitchhiking places ER architecture under the control of LE/Ly trafficking, implying multiple physiological consequences. For instance, access to the calcium ion stores in the ER may become subject to late endosomal/lysosomal transport regulation (van der Kant & Neefjes, 2014). This could possibly take place, during protrusion formation, where LE/Ly are directed to the sites of membrane expansion to provide membrane materials. At the same time, the ER is required here for calcium supply and ER hitchhiking could help to couple both processes (Goyal & Blackstone, 2013; Raffaello et al, 2016). Also, any process affecting LE/Ly trafficking should affect the ER architecture. These include starvation and cholesterol accumulation.

Here, we have shown that LE/Ly movements, ER dynamics, and the ER network architecture are intimately linked cell biological processes. When LE/Ly are tethered to the ER and proceed to move, the ER can remain tethered and hitchhike along with the moving LE/Ly (Fig 6). When proximity criteria are met, the hitchhiking ER tubule may fuse to another ER tubule to form a novel ER junction. Therefore, ER dynamics and structure are partially controlled by late endosomal transport, a process that in itself is regulated by various physiological conditions. Overall, we define ER hitchhiking with LE/Lys as a significant contributor to peripheral ER mobility and architecture.

# Materials and Methods

### Cell culture and constructs

COS7 cells (CRL-1651, ATCC, USA) were cultured in DMEM (Thermo Scientific, USA) supplemented with 10% FCS (Biowest, France). The cell line was regularly tested for mycoplasma contamination using MycoAlert™ Mycoplasma Detection Kit (Lonza, cat LT07-318).

A stable cell line of COS7 cells was generated using antibiotic pressure containing the transmembrane region of MOSPD2 with GFP fused to the N-terminus.

mScarlet -C1 and HA-C1 plasmids were described previously (Jongsma et al, 2020). GFP- and Scarlet-tagged MOSPD2 (IMAGE clone 4821861) transmembrane region was cloned into EGFP-C1 and mScarlet-C1 plasmids using 5'-CCCAGAATTCCGCAGAGAATC ACGCCCA-3' as forward primer and 5'-CCCAGGATCCTTACTGC TGGAACCAGATAC-3' as reverse primers and BamHI and HindIII restriction sites. TMEM55B (IMAGE clone 3940519) using 5'-CCCATGTACAAGATGGCGGCGGCAGATGGA-3' as forward primer and 5'-CCCACAATTGTCAGGAGAAGTTCTGGACAGGG-3' as reverse primer in EGFP-C1, mScarlet -C1 and 2xHA-C1 using BsrgI and MunI restriction sites. EGFP-Peroxisomes-0 and mCherry-KDEL were kind gifts from Michael Davidson (Addgene plasmid #55041, 54501; Rizzo et al, 2009). GFP-RILP was previously described and was cloned into mScarlet-C1 vector using HindIII and EcoRI restriction sites (Jordens et al, 2001). EB3-mGFP was a kind gift from Dr. Anna Akhmanova. GFP-RAB5, GFP-RAB7, GFP-RAB11, and GFP-RAB14 were produced as previously described (Kuijl et al, 2007; Kuijl et al, 2013; Sapmaz et al, 2019). mCherry-SEC61B, mCherry-CEPT1, and mCherry-PIS were gifts from Gia Voeltz (Addgene plasmid # 119078, 119079, 49155) (Zurek et al, 2011; English & Voeltz, 2013). GFP- SEC61B was a gift from Christine Mayr (Addgene

plasmid # 121159).(Ma & Mayr, 2018). pmScarlet_peroxisome_C1 was a gift from Dorus Gadella (Addgene plasmid # 85063 (Bindels et al, 2017).

### Antibodies and reagents

Following antibodies were used in this study: Rabbit anti-VAPA (Proteintech Cat#15275-1-AP), Rabbit anti-VAPB (Proteintech Cat# 14477-1-AP), Rabbit anti-KTN1 (Proteintech Cat#z19841-1-AP), Actin (Sigma-Aldrich Cat# A5441), Anti-Rabbit-HRP (Thermo Fisher Cat#G-21234), and Anti-Mouse-HRP (Thermo Fisher Cat#G-21040). To inhibit microtubule (de)polymerization, tissue culture medium was supplemented with 2 µM of paclitaxel for two hours (Merck, USA) in DMSO. The late endosomal/lysosomal compartment was visualized using SiR-lysosome at a concentration of 1 µM (Stein am Rhein, Switzerland). To ensure adequate retention of SiR-lysosome, cells were treated with 10 µM Verapamil as per manufacturer's recommendation. Mitochondria were labeled using Mitotracker Deep Red FM (Thermo Fischer, USA) at a concentration of 500 nM, as per manufacturers recommendation.

### Transfection

COS7 cells were transfected using Effectene (Qiagen, Germany) according to the manufacturer's instructions. For siRNA-mediated silencing, cells were reverse transfected with DharmaFECT transfection reagent #1 (Dharmacon, USA) and 50nM siRNA and samples were analyzed 72 hours later by confocal microscopy or qPCR. siRNAs were purchased from Dharmacon (USA) and were as follows: siVAPA (MQ-021382-01-0010), siVAPB (MQ-017795-0010), siMOSPD2 (MQ-017039-010), and siKinectin (MQ-010605-01-0005).

### cDNA synthesis and qPCR

RNA isolation, complementary DNA synthesis, and quantitative PCR with reverse transcription were performed according to the manufacturer's instructions (Roche, Switzerland). Signal was normalized to GAPDH and calculated using the pfaffl formula. Primers used for detection of GAPDH, VAPA, VAPB, and MOSPD2 were as follows: GAPDH forward: 5'-TGTTGCCATCAATGACCCCTT −3' and reverse 5'-CTCCACGACGTACTCAGCG −3'. VAPA forward 5' – AATGCTAC AGCCCTTTGACTATG – 3' and reverse 5' – TCATCAGGTTTTGCCTC TTTCC −3'. VAPB forward 5' – AGATGGACTGCGGATGAGGAA −3' and reverse 5' – CAGTTGGGGCTAGCGCTGAAA −3' and MOSPD2 forward 5' – ATGCTCGATGAGAGTTTTCAGTG −3' and reverse 5'-CCAACCAGAATGCTATGAGCTTC-3'. Kinectin-1 forward 5' – AAAT GTCTTCGTAGACGAACCCC −3' and reverse 5' – TTTGCAGTTTCA GTCTTCAGTT −3'.

### Microscopy

Cells were seeded in 35 mm glass bottom tissue culture dishes (MatTek, USA) or in 35 mm glass bottom tissue culture dish with 4 compartments (Greiner, Austria). Image acquisition was performed by an Andor Dragonfly 505 spinning disk confocal on a Leica DMi8 microscope with an Andor iXon Life 888 EMCCD camera and Andor Zyla 4.2 + sCMOS camera using a 565 nm long pass dichroic image splitter. (Oxford, UK). The microscopy set-up allowed for the

simultaneous acquisition of two channels. For live cell imaging, the microscopes were equipped with a humidified climate control system at 37°C supplemented with 5% $CO_2$. Specific frame rates are noted at the relevant experiments.

For fixed cell imaging, cells were seeded on glass coverslips and transfected. The day after transfections, cells were washed with PBS and fixed in 3.7% (w/v) formaldehyde in PBS solution for 10 min at RT. Next, cells were washed and mounted. Samples were imaged using a Leica TCS SP8 microscope (Leica Microsystems, Wetzlar, Germany) equipped with 405/488/561/647 nm laser lines. Images were analyzed using ImageJ Software.

### Membrane displacement analysis

To quantify membrane displacements of heterogeneously shaped membranes, we developed a membrane displacement analysis (MDA) method. This analysis method is for a large part based on optical flow analysis, which identifies corresponding areas between two frames and generates a vector flow map(Horne, 1981). This type of map describes frame-to-frame movement of local image areas. The vector flow map is visualized by color-coding the image frame by the magnitude of each flow vector (Fig 1B, panel II). In a parallel step, also (noisy) background pixels are matched from frame to frame. To mitigate these erroneous flow vectors, the flow vectors are based on the labeled membranes (Fig 1B, panel III). The masked vector flow maps reflect the end-point degree of displacement of labeled membranes between two images (Fig 1B, panel IV). By overlaying this with the original image acquisition, sequences are generated where the extent of movement of a membrane acquired was reflected by color intensity. The higher the color intensity, the further that pixel will have moved in relation to the previous image (Fig 1B, panel V). These data are then quantified in terms of fractions of membrane mobility. Using this quantification, the fraction of membrane movement can be determined (Fig 1B, panel VI). MDA has implemented the described membrane displacement analysis (MDA) as an ImageJ/Fiji plugin. Core functionality relies on the Gaussian Window MSE plugin by Stephan Saalfeld and Pavel Tomancak. Masking was performed using an automatic threshold of the image intensities after median filtering. The MDA plugin is available upon request with m.spits@lumc.nl or l.m.voortman@lumc.nl.

### ER junction analysis

ER junction analysis was performed by generating a mask of the ER using the auto local thresholding algorithm Phansalkar (Fig 4A, panel I). Next, a skeleton in generated from the ER mask (Fig 4A, panel II). This skeleton representation of the ER is then analyzed for the number of junctions (fig 4A, panel III) (Arganda-Carreras *et al*, 2010). The number of junctions is then divided by the analyzed surface area in $\mu m^2$. The ER junction analysis plugin for ImageJ is available upon request with m.spits@lumc.nl or l.m.voortman@lumc.nl

### Western blotting

siRNA-transfected COS7 cells were lysed in ice-cold lysis buffer (0.5% (v/v) NP-40, 50mM Tris–HCl 8.0, 150mM NaCl, 0.1% SDS and complete™ Protease Inhibitor Cocktail) and lysates were mixed with 2xSDS sample buffer (20% glycerol, 2% SDS, 125 mM Tris–HCl pH 6.8 and 0.002% (w/v) Bromophenol Blue). Samples were incubated at 95°C for 10 min. Proteins were separated by SDS–PAGE and transferred to nitrocellulose membranes. Membranes were blocked overnight with 5% (w/v) milk in PBST (PBS containing 0.05% (v/v) Tween 20), incubated with primary antibody solution in PBST, washed thrice with PBST, incubated with secondary antibody solution in PBST, washed thrice with PBST and twice with PBS before imaging. For detection, membranes were incubated with the substrate and imaged using Amersham Imager 600 (GE Healthcare).

### Statistics

All error bars correspond to standard deviation. Statistical evaluations report on Student's *t*-test as described in corresponding figure legends. *$P < 0.05$, **$P < 0.01$, ***$P < 0.001$, ****$P < 0.0001$, ns = not significant.

## Data availability

This study includes no data deposited in external repositories.

**Expanded View** for this article is available online.

## Author contributions

MS designed the study with input from JN. MS performed and analyzed nearly all experiments with help from ITH. BC and JJA provided technical support. MS and LMV designed the macro to analyze ER movement. MS designed the macro to analyze ER junctions. RHW performed and analyzed all qPCR experiments. MS wrote the manuscript with input from JN and BC. JN and MS coordinated the study.

## Conflict of interest

The authors declare that they have no conflict of interest.

## References

Arganda-Carreras I, Fernandez-Gonzalez R, Munoz-Barrutia A, Ortiz-De-Solorzano C (2010) 3D reconstruction of histological sections: Application to mammary gland tissue. *Microsc Res Tech* 73: 1019–1029

Bakker J, Spits M, Neefjes J, Berlin I (2017) The EGFR odyssey - from activation to destruction in space and time. *J Cell Sci* 130: 4087–4096

Bhaskara RM, Grumati P, Garcia-Pardo J, Kalayil S, Covarrubias-Pinto A, Chen W, Kudryashev M, Dikic I, Hummer G (2019) Curvature induction and membrane remodeling by FAM134B reticulon homology domain assist selective ER-phagy. *Nat Commun* 10: 2370

Bindels DS, Haarbosch L, van Weeren L, Postma M, Wiese KE, Mastop M, Aumonier S, Gotthard G, Royant A, Hink MA *et al* (2017) mScarlet: a bright monomeric red fluorescent protein for cellular imaging. *Nat Methods* 14: 53–56

Bola B, Allan V (2009) How and why does the endoplasmic reticulum move? *Biochem Soc Trans* 37: 961–965

Cabukusta B, Neefjes J (2018) Mechanisms of lysosomal positioning and movement. *Traffic* 19: 761–769

Chen S, Desai T, McNew JA, Gerard P, Novick PJ, Ferro-Novick S (2015) Lunapark stabilizes nascent three-way junctions in the endoplasmic reticulum. *Proc Natl Acad Sci U S A* 112: 418–423

Di Mattia T, Wilhelm LP, Ikhlef S, Wendling C, Spehner D, Nomine Y, Giordano F, Mathelin C, Drin G, Tomasetto C *et al* (2018) Identification of MOSPD2, a novel scaffold for endoplasmic reticulum membrane contact sites. *EMBO Rep* 19: e45453

Elliott T, Neefjes J (2006) The complex route to MHC class I-peptide complexes. *Cell* 127: 249–251

English AR, Voeltz GK (2013) Rab10 GTPase regulates ER dynamics and morphology. *Nat Cell Biol* 15: 169–178

English AR, Zurek N, Voeltz GK (2009) Peripheral ER structure and function. *Curr Opin Cell Biol* 21: 596–602

Friedman JR, Dibenedetto JR, West M, Rowland AA, Voeltz GK (2013) Endoplasmic reticulum-endosome contact increases as endosomes traffic and mature. *Mol Biol Cell* 24: 1030–1040

Friedman JR, Webster BM, Mastronarde DN, Verhey KJ, Voeltz GK (2010) ER sliding dynamics and ER-mitochondrial contacts occur on acetylated microtubules. *J Cell Biol* 190: 363–375

Goyal U, Blackstone C (2013) Untangling the web: mechanisms underlying ER network formation. *Biochim Biophys Acta* 1833: 2492–2498

Grigoriev I, Gouveia SM, van der Vaart B, Demmers J, Smyth JT, Honnappa S, Splinter D, Steinmetz MO, Putney Jr JW, Hoogenraad CC *et al* (2008) STIM1 is a MT-plus-end-tracking protein involved in remodeling of the ER. *Curr Biol* 18: 177–182

Guimaraes SC, Schuster M, Bielska E, Dagdas G, Kilaru S, Meadows BR, Schrader M, Steinberg G (2015) Peroxisomes, lipid droplets, and endoplasmic reticulum "hitchhike" on motile early endosomes. *J Cell Biol* 211: 945–954

Guo Y, Li D, Zhang S, Yang Y, Liu JJ, Wang X, Liu C, Milkie DE, Moore RP, Tulu US *et al* (2018) Visualizing Intracellular Organelle and Cytoskeletal Interactions at Nanoscale Resolution on Millisecond Timescales. *Cell* 175: 1430–1442

Horne DF (1981) Optical scales, reticles, gratings, masks, and standards. *Appl Opt* 20: 4000–4008

Horwitz SB (1994) Taxol (paclitaxel): mechanisms of action. *Ann Oncol* 5(Suppl 6): S3–S6

Hoyer MJ, Chitwood PJ, Ebmeier CC, Striepen JF, Qi RZ, Old WM, Voeltz GK (2018) A Novel Class of ER Membrane Proteins Regulates ER-Associated Endosome Fission. *Cell* 175: 254–265

Jongsma ML, Bakker J, Cabukusta B, Liv N, van Elsland D, Fermie J, Akkermans JL, Kuijl C, van der Zanden SY, Janssen L *et al* (2020) SKIP-HOPS recruits TBC1D15 for a Rab7-to-Arl8b identity switch to control late endosome transport. *EMBO J* 39: e102301

Jongsma ML, Berlin I, Wijdeven RH, Janssen L, Janssen GM, Garstka MA, Janssen H, Mensink M, van Veelen PA, Spaapen RM *et al* (2016) An ER-Associated Pathway Defines Endosomal Architecture for Controlled Cargo Transport. *Cell* 166: 152–166

Jordens I, Fernandez-Borja M, Marsman M, Dusseljee S, Janssen L, Calafat J, Janssen H, Wubbolts R, Neefjes J (2001) The Rab7 effector protein RILP controls lysosomal transport by inducing the recruitment of dynein-dynactin motors. *Curr Biol* 11: 1680–1685

Junutula JR, De Maziere AM, Peden AA, Ervin KE, Advani RJ, van Dijk SM, Klumperman J, Scheller RH (2004) Rab14 is involved in membrane

trafficking between the Golgi complex and endosomes. *Mol Biol Cell* 15: 2218–2229

van der Kant R, Fish A, Janssen L, Janssen H, Krom S, Ho N, Brummelkamp T, Carette J, Rocha N, Neefjes J (2013) Late endosomal transport and tethering are coupled processes controlled by RILP and the cholesterol sensor ORP1L. *J Cell Sci* 126: 3462–3474

van der Kant R, Neefjes J (2014) Small regulators, major consequences - Ca(2)(+) and cholesterol at the endosome-ER interface. *J Cell Sci* 127: 929–938

Kuijl C, Pilli M, Alahari SK, Janssen H, Khoo PS, Ervin KE, Calero M, Jonnalagadda S, Scheller RH, Neefjes J *et al* (2013) Rac and Rab GTPases dual effector Nischarin regulates vesicle maturation to facilitate survival of intracellular bacteria. *EMBO J* 32: 713–727

Kuijl C, Savage ND, Marsman M, Tuin AW, Janssen L, Egan DA, Ketema M, van den Nieuwendijk R, van den Eeden SJ, Geluk A *et al* (2007) Intracellular bacterial growth is controlled by a kinase network around PKB/AKT1. *Nature* 450: 725–730

Langemeyer L, Frohlich F, Ungermann C (2018) Rab GTPase Function in Endosome and Lysosome Biogenesis. *Trends Cell Biol* 28: 957–970

Lin S, Sun S, Hu J (2012) Molecular basis for sculpting the endoplasmic reticulum membrane. *Int J Biochem Cell Biol* 44: 1436–1443

Ma W, Mayr C (2018) A Membraneless Organelle Associated with the Endoplasmic Reticulum Enables 3'UTR-Mediated Protein-Protein Interactions. *Cell* 175: 1492–1506

Mogre SS, Christensen JR, Niman CS, Reck-Peterson SL, Koslover EF (2020) Hitching a ride: mechanics of transport initiation through linker-mediated hitchhiking. *Biophys J* 118: 1357–1369

Murphy SE, Levine TP (2016) VAP, a Versatile Access Point for the Endoplasmic Reticulum: Review and analysis of FFAT-like motifs in the VAPome. *Biochim Biophys Acta* 1861: 952–961

Raffaello A, Mammucari C, Gherardi G, Rizzuto R (2016) Calcium at the Center of Cell Signaling: Interplay between Endoplasmic Reticulum, Mitochondria, and Lysosomes. *Trends Biochem Sci* 41: 1035–1049

Raiborg C, Wenzel EM, Pedersen NM, Stenmark H (2016) ER-endosome contact sites in endosome positioning and protrusion outgrowth. *Biochem Soc Trans* 44: 441–446

Rizzo MA, Davidson MW, Piston DW (2009) Fluorescent protein tracking and detection: applications using fluorescent proteins in living cells. *Cold Spring Harb Protoc* 2009: pdb.top64.

Rocha N, Kuijl C, van der Kant R, Janssen L, Houben D, Janssen H, Zwart W, Neefjes J (2009) Cholesterol sensor ORP1L contacts the ER protein VAP to control Rab7-RILP-p150 Glued and late endosome positioning. *J Cell Biol* 185: 1209–1225

Rowland AA, Chitwood PJ, Phillips MJ, Voeltz GK (2014) ER contact sites define the position and timing of endosome fission. *Cell* 159: 1027–1041

Salogiannis J, Egan MJ, Reck-Peterson SL (2016) Peroxisomes move by hitchhiking on early endosomes using the novel linker protein PxdA. *J Cell Biol* 212: 289–296

Salogiannis J, Reck-Peterson SL (2017) Hitchhiking: A Non-Canonical Mode of Microtubule-Based Transport. *Trends Cell Biol* 27: 141–150

Santama N, Er CP, Ong LL, Yu H (2004) Distribution and functions of kinectin isoforms. *J Cell Sci* 117: 4537–4549

Sapmaz A, Berlin I, Bos E, Wijdeven RH, Janssen H, Konietzny R, Akkermans JJ, Erson-Bensan AE, Koning RI, Kessler BM *et al* (2019) USP32 regulates late endosomal transport and recycling through deubiquitylation of Rab7. *Nat Commun* 10: 1454

Ullrich O, Reinsch S, Urbe S, Zerial M, Parton RG (1996) Rab11 regulates recycling through the pericentriolar recycling endosome. *J Cell Biol* 135: 913−924

Wang S, Tukachinsky H, Romano FB, Rapoport TA (2016) Cooperation of the ER-shaping proteins atlastin, lunapark, and reticulons to generate a tubular membrane network. *Elife* 5: e18605

Wijdeven RH, Janssen H, Nahidiazar L, Janssen L, Jalink K, Berlin I, Neefjes J (2016) Cholesterol and ORP1L-mediated ER contact sites control autophagosome transport and fusion with the endocytic pathway. *Nat Commun* 7: 11808

Willett R, Martina JA, Zewe JP, Wills R, Hammond GRV, Puertollano R (2017) TFEB regulates lysosomal positioning by modulating TMEM55B expression and JIP4 recruitment to lysosomes. *Nat Commun* 8: 1580

van de Willige D, Hoogenraad CC, Akhmanova A (2016) Microtubule plus-end tracking proteins in neuronal development. *Cell Mol Life Sci* 73: 2053−2077

Zajac AL, Goldman YE, Holzbaur EL, Ostap EM (2013) Local cytoskeletal and organelle interactions impact molecular-motor- driven early endosomal trafficking. *Curr Biol* 23: 1173−1180

Zhao YG, Liu N, Miao G, Chen Y, Zhao H, Zhang H (2018) The ER Contact Proteins VAPA/B Interact with Multiple Autophagy Proteins to Modulate Autophagosome Biogenesis. *Curr Biol* 28(1234−1245): e1234

Zhou X, He Y, Huang X, Guo Y, Li D, Hu J (2019) Reciprocal regulation between lunapark and atlastin facilitates ER three-way junction formation. *Protein Cell* 10: 510−525

Zulkefli KL, Houghton FJ, Gosavi P, Gleeson PA (2019) A role for Rab11 in the homeostasis of the endosome-lysosomal pathway. *Exp Cell Res* 380: 55−68

Zurek N, Sparks L, Voeltz G (2011) Reticulon short hairpin transmembrane domains are used to shape ER tubules. *Traffic* 12: 28−41